Article:
Song, Y, Wang, Y, Jin, L et al. (2022) Quantitative contribution of the Grain for Green project to vegetation greening and its spatiotemporal variation across the Chinese Loess Plateau. Land Degradation and Development, 33 (11). pp. 1878-1891. ISSN: 1085-3278

https://doi.org/10.1002/ldr.4269

Quantitative contribution of the Grain for Green project to vegetation greening and its spatiotemporal variation across the Chinese Loess Plateau

Yi Song[1, 2], Yunqiang Wang[1, 2 *], Long Jin[3], Weiyu Shi[4], Jagannath Aryal[5], Alexis Comber[6]

[1] State Key Laboratory of Loess and Quaternary Geology, Institute of Earth Environment, Chinese Academy of Sciences, Xi'an 710061, China

[2] CAS Center for Excellence in Quaternary Science and Global Change, Xi'an, 710061, China

[3] College of Civil Engineering, Xi'an University of Science and Technology, Xi'an 710065, China

[4] School of Geographical Sciences, Southwest University, Chongqing 400715, China

[5] Faculty of Engineering and IT, Department of Infrastructure Engineering, University of Melbourne, Parkville, Victoria, Australia

[6] School of Geography, University of Leeds, Leeds, LS2 9JT, United Kingdom

* Corresponding author, E-mail address: wangyq@ieecas.cn (Y. Wang)

Running title: Contribution of the Grain for Green project to vegetation greening

Abstract: A distinct greening trend is evident in Asia, especially on the Loess Plateau (LP) of China, which is driven by climate change and large-scale land-use-related ecological projects, especially the "Grain for Green" project (GFGP). However, the specific contributions of the GFGP to vegetation greening and their variation characteristics at a large spatiotemporal scale are not yet clear. We used long-time-series normalized difference vegetation index (NDVI) datasets and climate datasets based on the double mass curve (DMC) method to quantify the contributions of ecological projects and climate change to the greening trend on the LP. We found that the interannual fluctuation of vegetation change was likely related to the interannual fluctuation of climate, especially precipitation. The increasing trend of vegetation change after 2005 indicated that the GFGP, as a type of external disturbance, began to improve vegetation growth. The GFGP failed initially to make a positive contribution in the first few years because of the drought conditions in 1999 and 2005. The increased precipitation played a critical role in enhancing the output of the GFGP on the LP after 2005. Then, the contribution of the GFGP increased quickly until 2013, after which it remained stable and reached average values of 58.8%±19.34% and 31.7%±24.3% in the representative areas that conducted the GFGP and in other regions with a lower implementation intensity of the GFGP, respectively. Our results highlighted that the contribution of GFGP had spatiotemporal variation due to the spatial heterogeneity of the project intensity and the effect of forest stand age.

Keywords: the Loess Plateau; vegetation dynamics; Grain for Green project; precipitation change; quantification of contributions

1. Introduction

Vegetation accounts for the main part of terrestrial ecosystems and plays a key role in the flows of matter and energy among the pedosphere, hydrosphere and atmosphere and, thus, in regulating the climate of the Earth (J. Chen et al., 2019; Hu, Fu, Liu, Jin, & Guo, 2010; Peng et al., 2014; S. Piao, Fang, & He, 2006). Changes in vegetation greenness have been reported widely at regional and global scales based on forest inventory and satellite images (C. Chen et al., 2019; Myneni, Keeling, Tucker, Asrar, & Nemani, 1997; Shilong Piao et al., 2015; Zhu et al., 2016). The main causes of such changes have recently been recognized as the changes in climate conditions and atmospheric composition as well as land-use-related human activities (Hansen et al., 2013; Herrmann, Anyamba, & Tucker, 2005; L. Xu et al., 2013); however, nonlinear effects and interactions of these drivers make it challenging to quantify their individual contributions to observed vegetation greenness change, and the results have a large amount of uncertainty (B. Chen et al., 2014; Shilong Piao et al., 2020).

The Loess Plateau (LP) in China (~640,000 km^2) is the largest area of loess deposition in the world and is considered a global focus of studies of land degradation and ecosystem fragility due to its serious soil erosion (Gao, Ma, & Fu, 2016; Q. Liu, Wang, Zhang, & Chen, 2013). To halt soil erosion and improve ecosystem services, the Chinese government implemented the "Grain for Green" project (GFGP) in 1999 (Yifei Wang & Yao, 2019), which was widely promoted after 2002 (S. Cao, Li, & Yu, 2009). To date, the GFGP is the largest land-use-related ecological project in China and even worldwide (Deng, Shangguan, & Sweeney, 2014), and it has greatly increased the vegetation cover on the LP (B. Zhang, He, Burnham, & Zhang, 2016).

Since 2000, China has accounted for 25% of the global net increase in leaf area but has only 6.6% of the global vegetated area (C. Chen et al., 2019). According to time series satellite monitoring data, the LP represents a typical region of vegetation increase in China (Grogan, Pflugmacher, Hostert, Verbesselt, & Fensholt, 2016; Hansen et al., 2013). After the launch of the GFGP, many studies using remotely sensed images confirmed a widespread increase in vegetation on the LP (Z. Cao, Li, Liu, Chen, & Wang, 2018; Shuai Li et al., 2016; Sun et al., 2015). For example, 48,300 km^2 of farmland was converted to forest and grassland between 2000 and 2008 (Lü et al., 2012); vegetation cover nearly doubled from 1999 to 2013, increasing from 31.6% to 59.6% (Y. Chen et al., 2015); and forest area increased by approximately 49,000 km^2 from 2001 to 2016 (Yuhang Wang et al., 2018). These findings indicated where and when the LP "turned green". Long-term vegetation changes are driven by multiple interacting biogeochemical drivers (X. Wang et al., 2014) and human-induced land-use changes (Mendoza-Ponce, Corona-Nunez, Kraxner, Leduc, & Patrizio, 2018). The biogeochemical drivers mainly include climate change (Y. Zhang et al., 2014), the fertilization effects of elevated CO_2 concentrations (Los, 2013) and varying rates of nitrogen deposition (Dalal, Thornton, Allen, & Kopittke, 2021); in contrast, the human-induced land-use changes mainly include afforestation, deforestation, and grazing. The dominant drivers of vegetation change vary from place to place (Zhu et al., 2016). According to some previous studies, the dominant drivers of the vegetation greening trend on the LP after 2000 were climate change and ecological projects (Z. Cao et al., 2018; Xiao, 2014), rather than the changes in atmospheric composition (Z. Liu, Wang, Wang, & Wang, 2020; Xie, Mo, Hu, & Liu, 2020). A few studies have investigated the specific contribution of the GFGP to the vegetation increase on the LP

(Zheng et al., 2019). However, several important scientific issues, such as the variation characteristics of the contributions of the GFGP at spatiotemporal scales, need increasingly to be clarified. Actually, the implementation intensity of the GFGP had spatial heterogeneity, and the effect of afforestation varied with forest stand age. Accordingly, we hypothesize that (i) the contribution of the GFGP to vegetation increases shows spatial heterogeneity and temporal variability on the LP, and (ii) the GFGP contribute more to vegetation increases than does climate change in some representative areas that have conducted GFGP. To test these two hypotheses, the objectives of this study were to (1) investigate the spatiotemporal characteristics of vegetation change across the LP from 1982 to 2019 using multisource satellite data; and (2) quantify the contribution of the GFGP to vegetation changes and explore the spatiotemporal variation of such impacts on the LP.

2. Materials and Methods

2.1 Data and data preprocessing

Two normalized difference vegetation index (NDVI) datasets from the Advanced Very High Resolution Radiometer (AVHRR) that covered the period of 1982 to 2015 and the Moderate Resolution Imaging Spectroradiometer (MODIS) that covered the period of 2001 to 2019 were used in our study. The AVHRR Global Inventory Modeling and Mapping Studies (GIMMS) NDVI dataset was obtained from NASA (https://ecocast.arc.nasa.gov/). The MODIS NDVI dataset (MOD13Q1) was obtained from the Land Processes Distributed Active Archive Center (LPDAAC) of NASA (https://lpdaac.usgs.gov/).

The AVHRR GIMMS NDVI dataset and the MODIS MOD13Q1 NDVI dataset have temporal resolutions of 15 days and 16 days, respectively. In the current study, we used the

seasonally integrated NDVI (SINDVI) to analyze the vegetation change since 1982. The SINDVI was defined as the sum of the NDVI values that exceeded the critical value of NDVI > 0.1 for each pixel during the whole year, because the NDVI increases from 0.1 to 1.0 with increasing amounts of vegetation greenness (Stow et al., 2003). Compared to the maximum NDVI during a year, the SINDVI could enhance the annual variability in the NDVI time series at pixel scale (Y. Song, Jin, & Wang, 2018). Then, we used the cumulative SINDVI (CSINDVI) to quantify the contribution of the GFGP to the vegetation increase at different spatial scales. The CSINDVI was defined as the cumulative value of the SINDVI of all pixels within a certain quadrat (see the quadrat design description in Section 2.2). Compared to the mean value of SINDVI within a certain area, the CSINDVI enhanced the annual variability in areas with sparse vegetation, because the average SINDVI values would be weakened by the low SINDVI values of sparse vegetation (Supplementary Fig. S1).

Monthly temperature and precipitation data from 62 national meteorological stations (NMSs) covering 1981 to 2019 (Fig. 1) were used. The names of the 62 NMSs are listed in Supplementary Table S1. The meteorological data were obtained from the National Meteorological Information Center (NMIC) of the China Meteorological Administration (CMA) (http://data.cma.cn/).

Insert Fig. 1

On the LP, the start of the growing season generally occurs in early spring (April) and ends in late fall (October) (Sun et al., 2015; H. Wang et al., 2016). Climate changes in the growing season affect vegetation growth in the same year, while in the dormancy period (November to March) affect vegetation growth in the following year (Guo et al., 2017). Thus,

we calculated the annual precipitation (P) and the annual average temperature (T) using monthly meteorological records from November to October of the following year for all 62 NMSs on the LP.

2.2 Quadrat design

We selected 28 NMSs located far from towns and cities from all 62 NMSs on the LP. Of the 28 selected NMSs, two were located in Qinghai Province, eight were located in Gansu Province, seven were located in Shaanxi Province, six were located in Ningxia Province, four were located in Shanxi Province, and one was located in the Inner Mongolia Autonomous Region (Fig. 1). We designed 3 nested quadrats with different sizes around each of the 28 NMSs. The sizes of the quadrats ranged from 1 × 1 pixel to 3 × 3 pixels of the GIMMS NDVI image (8 × 8 km to 24 × 24 km). Then, GIMMS CSINDVIs were calculated within each of the nested quadrats to quantify the impacts of climate factors and the GFGP on vegetation changes (see Section 2.4: Quantification of contribution).

2.3 Significance of changes in vegetation and climate

The significance of changes in vegetation (Sig_{SINDVI}) and two climate factors, P (Sig_P) and T (Sig_T), was assessed using the Mann-Kendall test, which is a nonparametric statistical test that is widely used to detect trends in hydrological, climatic and environmental factors (Sicard, Mangin, Hebel, & Malléa, 2010; B. Zhang et al., 2016). The confidence level of α was set to 0.1, 0.05, 0.01, or 0.005 in the current study.

2.4 Quantification of contribution

Human induced land use cover change plays a crucial role in global environmental change (Mendoza-Ponce et al., 2018). In the current study, we used the double mass curve (DMC)

method to quantify the contribution of the GFGP to vegetation changes (*CONTRIBUTION*_GFGP). A DMC is defined as a plot of the cumulative values of one variable against the cumulative values of another variable over the same time span, and this method is typically used for precipitation and various other types of hydrological data, such as reservoir sedimentation (Yang et al., 2017) and sediment transport (Kisi & Ay, 2014; S. Wang et al., 2016). The slope of the DMC represents the constant of proportionality between the two quantities, and a break in the slope indicates a change in the constant of proportionality.

Since DMC worked only for two variables, we first used a linear regression method to combine the two climate variables (precipitation and temperature) into an integrated climate index (CI). The CI was calculated as follows:

$$\mathrm{CI} = a \times P + b \times T + c, \quad (1)$$

where a and b are the standard regression coefficients for P and T, respectively.

The AVHRR NDVI dataset has a longer time series than MODIS NDVI dataset. The observations of 19 years before the implementation of the GFGP can be used to fit the linear relationship between the cumulative CI (CCI) and the cumulative CSINDVI (CCSINDVI). This linear relationship indicated the original interactive relationship of vegetation and climate (IR_{VC}) before the implementation of the GFGP. However, the MODIS NDVI dataset has been collected since 2000, so no data could be used to determine the original IR_{VC} before the implementation of the GFGP. Thus, the AVHRR NDVI dataset was more suitable than the MODIS NDVI dataset for the quantification of *CONTRIBUTION*_GFGP.

According to the principle of DMC method, only when the correlations between the CSINDVI and CI were significantly positive (the confidence level was set to 0.05) could

*CONTRIBUTION*_GFGP be calculated using the DMC method. Therefore, we first calculated the correlations between the CSINDVI and CI to ensure the proportional relationship between the two quantities. Here we took the contribution quantification around Suide (SD) NMS as an example. The correlation coefficient between the CI and CSINDVI for the SD quadrat of 16 × 16 km was 0.526, which was significant at the confidence level of 0.01. The DMC for the quadrat of 16 × 16 km around SD NMS is shown in Fig. 2. The CCI and CCSINDVI values in the k^{th} year (CCI_k and $CCSINDVI_k$) were calculated as follows:

$$\mathrm{CCI}_k = \sum_{j=1982}^{k} \mathrm{CI}_j, \tag{2}$$

$$\mathrm{CCSINDVI}_k = \sum_{j=1982}^{k} \mathrm{CSINDVI}_j, \tag{3}$$

The scatters of the CCI and CCSINDVI depicted a straight light until 2001 (the gray square dots in Fig. 2). This means that the implementation of the GFGP, as an external disturbance, changed the original IR_{VC} after 2000. Thus, we determined the original IR_{VC} before the implementation of the GFGP using the data from 1982 to 2000 (the red line in Fig. 2). The R^2 value of the linear regression relationship was greater than 0.9999. Then, the estimates of the $CCSINDVI_k$ after 2000 ($ECCSINDVI_k$, k>2000) were calculated based on the original IR_{VC}, which indicated a virtual value of $CCSINDVI_k$ that was not affected by the GFGP (the red dots in Fig. 2). The change in $CCSINDVI_k$ caused by the GFGP ($\Delta CCSINDVI\_GFGP_k$) could be calculated as follows:

$$\Delta\mathrm{CCSINDVI\_GFGP}_k = \mathrm{CCSINDVI}_k - \mathrm{ECCSINDVI}_k. \tag{4}$$

The *CONTRIBUTION*_GFGP (k>2000) could be quantified as the percentage of the change in $CCSINDVI_k$ caused by the GFGP out of all changes in the $CCSINDVI_k$ caused by climate ($\Delta CCSINDVI\_CI_k$) and the GFGP. To calculate the $\Delta CCSINDVI\_CI_k$, we designed an ideal

situation in which the climate (CI) would remain stable (as a constant) and cause no changes in vegetation (CSINDVI) after 2000. In the current study, we used the mean value of CI from 1982 to 2000 ($mean_{j=1982}^{2000} CI_j$) as the constant in the ideal situation. The ideal CCI ($ICCI_k$, k>2000) could be calculated as follows:

$$\mathrm{ICCI}_k = \sum_{j=1982}^{2000} CI_j + (k - 2000) \times mean_{j=1982}^{2000} CI_j. \quad (5)$$

The ideal values of CCI and CCSINDVI ($ICCI_k$ and $ICCSINDVI_k$, k>2000) should follow the original IR_{VC} as well. Thus, we estimated the $ICCSINDVI_k$ (k>2000) using the $ICCI_k$ (the blue diamonds in Fig. 2). The $\Delta CCSINDVI\_CI_k$ could be calculated as follows:

$$\Delta\mathrm{CCSINDVI\_CI}_k = \mathrm{ECCSINDVI}_k - \mathrm{ICCSINDVI}_k \quad (6)$$

Using this method, the *CONTRIBUTION*_GFGP around the other 27 NMSs at all three spatial scales (8×8 km, 16×16 km and 24×24 km) were calculated.

Insert Fig. 2

3. Results

3.1 Vegetation change on the LP from 1982 to 2019

The GFGP divided our study period into two phases. In the current study, we planned to use the MODIS NDVI to learn the significance of vegetation changes from 2001 to 2019 since the latest NDVI data (after 2015) was not available in AVHRR GIMMS NDVI dataset. However, the two NDVI datasets have a clear difference due to the two sensors' different spatial and spectral resolutions. We first calculated the Sig_{SINDVI} from 2001 to 2015 using AVHRR GIMMS NDVI dataset and MODIS NDVI dataset, respectively. The result (Supplementary Fig. S2) indicated that the Sig_{SINDVI} which were calculated using the AVHRR GIMMS NDVI

and the MODIS NDVI during the same time span have similar values and are comparable in terms of their characteristics of spatial patterns.

In the first 19-year phase (from 1982 to 2000), over 70% of the LP area was found to have nonsignificant changes at a confidence level (α) of 0.1 using the SINDVI. Vegetation in some areas in the center of the LP along the Yellow River and its tributary, the Luohe River, decreased significantly during these 19 years (Fig. 3a). In the second 19-year phase (from 2001 to 2019), almost 80% (79.1%) of the area of the LP showed a significant increase, with an α of 0.1, in the SINDVI. In addition, vegetation in more than 60% (60.7%) of the LP increased significantly, with an α of 0.005. The greatest increase occurred in the northern part of Shaanxi Province, a representative area that conducted the GFGP (Y. Chen et al., 2015). Within the second 19-year phase, the LP started to turn green gradually from 2000 (Supplementary Fig. S3). The annual maximal vegetation coverage (VC_{max}) of the representative area where the GFGP was conducted varied from 27.4% in 2000 to 57.5% in 2019 (calculated using MODIS MOD13Q1 NDVI).

Insert Fig. 3

3.2 Relationships between vegetation change and climate factors on the LP

We compared the troughs and peaks in the VC_{max} of the representative area where the GFGP was conducted (calculated using the AVHRR GIMMS NDVI) with those in P and T obtained by the 9 NMSs in this area (Fig. 4). The VC_{max} always displayed troughs (in 1987, 1989, 1991, 1997, 1999, 2005 and 2015) and peaks (in 1988, 1990, 1998, 2003, and 2013) in the same years as those in which the P values reached their minima and maxima, respectively. Some troughs (in 1992, 1993, and 2011) and peaks (in 2009 and 2013) in the VC_{max} matched

the minima and maxima of *T* as well. We obtained similar results by comparing the SINDVIs derived from the AVHRR GIMMS NDVI and MODIS MOD13Q1 NDVI datasets with *P* and *T* at the 28 NMSs on the LP (Supplementary Fig. S4). These results indicated that the interannual fluctuation of vegetation change was likely related to the interannual fluctuation of climate, especially that of precipitation. The main reason for this result is that the LP is characterized as only water source for the water-limited ecosystem of the LP (Yunqiang Wang, Shao, Zhu, Sun, & Fang, 2018) and thus vegetation is sensitive to precipitation (Jiang et al., 2019; W. Zhang et al., 2019). The GFGP was implemented on a large scale from 2002 to 2004 (Xiao, 2014). The VC_{max} increased significantly (with an α of 0.05) after 2005. Interestingly, the troughs and peaks in VC_{max} were still consistent with the minima and maxima of the two climate factors after 2005, although the trend of vegetation increases did not follow that of the two climate factors. This result indicated that the GFGP, as a type of external disturbance, affected the change in vegetation together with the two climate factors since 2000, especially after 2005.

Insert Fig. 4

3.3 Contribution of the GFGP to vegetation increase

The correlation coefficients between the CI and CSINDVI for almost all quadrats at 3 different spatial scales (8 × 8 km, 16 × 16 km, and 24 × 24 km) were significantly positive (with an α of 0.05), except the quadrat of Lintao (LT) at the 8 × 8 km scale (Table 1). The *CONTRIBUTION*_GFGP to vegetation changes was calculated using the CSINDVI, which was derived from the AVHRR GIMMS NDVI datasets based on the DMCs of the quadrats at the three different scales. The impact of the GFGP on the vegetation change is planar. According

to Table 1, the values of *CONTRIBUTION*_GFGP vary as the quadrat size (calculation scope) increases due to its spatial scale dependence. When the *CONTRIBUTION*_GFGP was calculated at a smaller quadrat size as 8 × 8 km, the *CONTRIBUTION*_GFGP are vulnerable to some random factors. Random factors may include the scale and heterogeneity of impacts arising from the GFGP, the relative position of the GFGP and the quadrats, and the spatial resolution of the satellite images. If the scope of the GFGP is much larger than the quadrat size, the effect of random factors will decrease as the quadrat size increases, and the values of *CONTRIBUTION*_GFGP will remain stable. Thus, the *CONTRIBUTION*_GFGP should be analyzed at a suitable spatial scale such that these random effects are eliminated and the *CONTRIBUTION*_GFGP is stable. Since the meteorological data involved in the calculation were at the point scale, the quadrat size cannot be increased without limit. In our study, only three spatial scales were analyzed: 8 × 8 km, 16 × 16 km, and 24 × 24 km. We observed that at 15 NMSs, such as Wuqi (WQ), Dingbian (DB), and Hengshan (HS), the CONTRIBUTION_GFGP values at the scales of 16 × 16 km were closer to those at 24 × 24 km than to those at 8 × 8 km (Table 1). At the other 13 NMSs, the gaps between the *CONTRIBUTION*_GFGP values at the three scales were similar. These results indicated that the larger scale as 24 × 24 km will be the suitable spatial scale affected by fewer random factors than the other two scales.

Insert Table 1

The intensity of the GFGP, varied from place to place. Farmlands on the LP with a slope greater than 15° were the target areas of the GFGP. These sloping farmlands are mainly distributed in northern Shaanxi (the representative area that conducted the GFGP). In this area,

the GFGP explained an average of 58.8%±19.34% of the vegetation increases at a 24 × 24 km spatial scale (Fig. 5, Table 1). This result verified our hypothesis (ii). However, in other areas, the *CONTRIBUTION*_GFGP values were lower and reached an average of only 31.7%±24.3% (at a 24 × 24 km spatial scale). Moreover, in some areas of Qinghai and Gansu Provinces where the GFGP was less intense, such as Guide (GD) and Jingtai (JT), the GFGP hardly contributed to vegetation increase (even less than 1%). The *CONTRIBUTION*_GFGP varied from place to place based on the intensity of the GFGP implementation, which verified our hypothesis (i) that *CONTRIBUTION*_GFGP had spatial heterogeneity. In addition, the outcomes of the GFGP (the increase in the CSINDVI, which was explained by the GFGP, ΔCSINDVI_GFGP) varied with precipitation. The regions with annual precipitation less than 400 mm, such as Yanchi (YanC) and Haiyuan (HY) had a lower ΔCSINDVI_GFGP than the regions with annual precipitation more than 400 mm, such as Suide (SD) and Xingxian (XingX), although the *CONTRIBUTION*_GFGP in the YanC and HY was greater (Table 2). Moreover, the increase in precipitation played a critical role in enhancing the outcome of the GFGP. For example, XingX and Lingtao (LT) has the similar annual precipitation, while the GFGP contributed similar positive efforts on vegetation greening in the two regions, however, the greater increases in *P* lead to a higher ΔCSINDVI_GFGP in XingX than in LT.

Insert Fig. 5

Insert Table 2

It should be noted that the effect of forest stand age was attributed to *CONTRIBUTION*_GFGP. The *CONTRIBUTION*_GFGP of 28 NMSs varied from 2002 to 2015 (Supplementary Table S2). The GFGP, did not have a positive effect on vegetation

growth until 2005 in XingX, 2006 in SD, 2008 in Luochuan (LC) and HS, and 2009 in DB, WQ, YanC, Yulin (YL), and Lishi (LS). Subsequently, the *CONTRIBUTION*_GFGP increased rapidly until 2013. As the speed and scope of the implementation of the GFGP decreased after 2012, the *CONTRIBUTION*_GFGP remained stable (Fig. 6; Supplementary Table S2). This result verified our hypothesis (i) that the *CONTRIBUTION*_GFGP varied over time.

Insert Fig. 6

4. Discussion

4.1 Interactions between vegetation and climate on the LP

The precipitation over mainland Asia is controlled by the Asian monsoon system, which brings warm moisture-bearing winds of maritime origin (Hanlin Wang et al., 2019). The East Asian summer monsoon (EASM) is the most important climate system over East Asia, and it provides approximately 60 ~ 70% of the annual mean precipitation over northern China (Lei, Hoskins, & Slingo, 2014). On the LP, the moisture of summer precipitation is mainly transported from the western Pacific Ocean driven by the EASM (C. Zhang et al., 2020), while in autumn, the interannual variability of precipitation is always affected by the high degree synergic air-sea interactions, ENSO and the Indian Ocean Dipole (IOD) (K. Xu, Zhu, & Wang, 2016). Some studies found that emissions of anthropogenic aerosols had the potential to weaken the EASM (as represented by precipitation) from 1934 to 2001 (Yu Liu et al., 2019; F. Song, Zhou, & Qian, 2014). After the drought from 1999 to 2000, the precipitation increased significantly over the LP (Fig. 7). Regarding the reasons that caused the increase in precipitation on the LP after 2000, some studies noted that anthropogenic greenhouse forcing caused the increase in summer precipitation after 2000 (Fasullo, 2012; Huang, Ren, Chadwick,

& Deng, 2021). In addition, the enhanced East Asian jet stream, which was caused by the anomalous upper-level anticyclone shifting northward, ascended over the LP and finally increased autumn precipitation (K. Xu et al., 2016). However, other studies noted that increased vegetation enhanced evapotranspiration and increased surface roughness, which further enhanced local moisture recycling and potentially increased local summer precipitation (Yongqiang Liu, Stanturf, & Lu, 2008; Xiao, 2014). The contributions of different forcings that affect the precipitation variation are subject to regional dependence. Huang et al. found that the increase in summer precipitation across the East Asian continent (especially over Central China) was mainly caused by the direct radiative effect of increasing CO_2 based on a set of time-slice experiments (Huang et al., 2021). Thus, we did not consider the feedback of increased vegetation to local precipitation because the plant physiological effect was not a remarkable forcing that increased the summer precipitation change over most parts of northern East Asia (Huang et al., 2021). The direct radiative effect of elevated CO_2 concentrations which drove the increase in precipitation after 2000 on the LP was considered in the current study. The fertilization effect of elevated CO_2 concentrations was not considered in the current study because it was not the dominant driver of vegetation greening on the LP (Z. Liu et al., 2020; Xie et al., 2020). The role of improving the water-use efficiency of plants (Lian et al., 2021; Zhu et al., 2016) of elevated CO_2 concentrations will be considered in our future studies.

Insert Fig. 7

Afforestation reduces albedo and increases ET and surface roughness, which causes a regional cooling effect (Davin & de Noblet-Ducoudré, 2010). After the implementation of the GFGP, the warming trend over the LP was relieved significantly (Fig. 7b and d).

4.2 Spatial heterogeneity and temporal variability of the contributions

Since the implementation of the GFGP, many studies have focused on the vegetation changes that have occurred. Xiao stated that the GFGP led to significant increases in the vegetation index and leaf area index and indicated that the vegetation cover increased by 41.0% (Xiao, 2014). Cao et al. found that the rate of the NDVI increase after 2000 was generally 6.3 times greater than that before 2000 over the whole LP, and significant increases were concentrated in areas where precipitation was greater than 400 mm (Z. Cao et al., 2018). Climate change and the implementation of the GFGP were considered the main reasons for the vegetation increases over the LP since 2000 (Xin, Xu, & Zheng, 2008). Some scientists noted that the GFGP resulted in a great contribution to vegetation increases (Y. Chen et al., 2015). Other studies using qualitative approaches determined that climate change contributed more to vegetation greening on the LP. For example, McVicar et al. noted that climate factors were critical for successful afforestation and restoration program outcomes (McVicar et al., 2007; McVicar et al., 2010). Li et al. noted that the vegetation increases in areas that implemented the GFGP were induced by increased precipitation during the later stage of the GFGP (Shuangshuang Li, Yang, Liu, Liu, & Shi, 2015). These results are partially consistent with the findings of our research. However, the specific contribution of increased precipitation is still unclear in the studies mentioned above.

According to our results, troughs in the VC_{max} time series occurred in 1987, 1989, 1991, 1997, 1999 and 2005 because P reached its minimum in these six years (Fig. 4). According to data from the National Bureau of Statistics, in the first few years of the GFGP (from 2002 to 2004), the annual afforestation area was the largest. However, the VC_{max} of the LP did not

increase immediately. During the implementation of the GFGP, the *P* of the LP increased greatly from 2006 to 2008 and from 2011 to 2013. Consequently, the VC_{max} of the LP increased greatly during these two periods of precipitation increase. The increase in precipitation served as a "catalyst" that accelerated the increasing trend in vegetation. Cao et al. noted that afforestation had a time-lag effect on the NDVI (Z. Cao et al., 2018). The likely reason for such a time lag was that vegetation was waiting for an opportunity to turn green associated with greater precipitation, which was verified in the current study.

How much did climate change and how much did the GFGP contribute to vegetation increases on the LP? A few quantitative studies have focused on this issue. For example, Zheng et al. used the NPP model to estimate the relative contributions of climate change and the GFGP and found that the two factors explained 57.7% and 42.3% of the vegetation increase on the LP, respectively (Zheng et al., 2019). Their results indicated that climate change contributed more to increases in vegetation on the LP since 2000 than did the GFGP. However, the current study verified that the contribution of the GFGP to vegetation increases showed distinct spatiotemporal variations. On the spatial scale, the GFGP explained an average of 58.8%±19.34% of the vegetation increases in the representative area that conducted the GFGP but contributed less to vegetation increases in other regions (less than did climate change). The outcome of the GFGP also varied from place to place according to the *P*. On the temporal scale, the GFGP did not make a positive contribution in the first few years because of the drought conditions during these years. Although more trees were planted from 2002 to 2004, the increase in greenness was limited by the lack of water availability. The GFGP began to make positive contributions after 2005 in most regions of the LP (Supplementary Table S2).

4.3 Effect of other ecological projects on vegetation increase

The *CONTRIBUTION*_GFGP calculated in the current study was the sum contribution of all ecological projects, including GFGP, terrace farming, and check dams. Terrace farming and check dams are two other typical ecological projects that have increased precipitation retention on the LP (Houjie Wang et al., 2007). These two long-accepted methods reduced sediment fluxes into river systems (S. Wang et al., 2016), and had a benefit of creating fertile, and flat agricultural land (S. Wang et al., 2016). These two projects lead to increases in subsequent increases in vegetation. The contribution of each project could not be quantified separately because these three ecological projects were consistently implemented in the same regions and had overlapping time spans with the GFGP. Terrace farming has been implemented on the LP since1950s. Check dams have been built on the LP since 1960s. More than 100 000 check dams have been built over the past several decades on the LP (Yafeng Wang, Fu, Chen, Lu, & Gao, 2011). Before 2000, these two ecological projects did not bring about significant vegetation increase in large areas as the GFGP did after 2000 (Fig. 2 and 3). Compared with the direct effect of the GFGP, however, the impacts caused by these two projects were more indirect. The scope of these two projects was not as extensive as that of the GFGP. Therefore, the contributions of these two projects to vegetation increase were much smaller than that of the GFGP (They were not even in an order of magnitude). The contribution calculated using the DMC method in the current study was mainly caused by the GFGP.

4.4 Sustainability of greening on the LP

The LP is in the Chinese arid and semi-arid region, where vegetation is very sensitive to water stress. According to our study, the outcome of the GFGP was determined by the local

rainfall as well as the intensity of the project. More water resource is required to sustain the greening, as the new artificial forests and shrubs had been planted during the implementation of GFGP. Feng et al., pointed out that the current amount of revegetation is approaching the limits of sustainable water resources (Feng et al., 2016). Some studies stated that artificial forests consumed more deep soil moisture than cultivated crops, which induced dry soil layer formation on the LP (Jia, Shao, Zhu, & Luo, 2017). Large-scale vegetation restoration has also aggravated water scarcity, gradually leading to soil desiccation (S. Wang, Fu, Gao, Yao, & Zhou, 2012). Therefore, to what extent can ecological projects improve vegetation depends on the ecological carrying capacity of local water resources.

5. Conclusion

We quantified the *CONTRIBUTION*_GFGP and analyzed its spatiotemporal variation across the LP. The *CONTRIBUTION*_GFGP values varied with the project intensity and the effect of forest stand age at the spatial and temporal scales. The GFGP contributed more to vegetation greening than does climate change in some representative areas that have conducted GFGP. However, in some areas where the annual precipitation was less than 400mm, even if the afforestation activities were more vigorous (*CONTRIBUTION*_GFGP>80%), the increase in vegetation greenness was still limited. The increased precipitation enhanced the output of the GFGP on the LP.

Data availability

The AVHRR Global Inventory Modeling and Mapping Studies (GIMMS) NDVI dataset was obtained from NASA (https://ecocast.arc.nasa.gov/). The MODIS NDVI dataset (MOD13Q1) was obtained from the Land Processes Distributed Active Archive Center (LPDAAC) of NASA (https://lpdaac.usgs.gov/). The meteorological data were obtained from the National

Meteorological Information Center (NMIC) of the China Meteorological Administration (CMA) (http://data.cma.cn/).

Acknowledgments

This research was supported by the National Key Research and Development Program of China (No. 2019YFA0607303), the National Natural Science Foundation of China (No. 41722106, 41571130083, 41530854 and 41977422), the Youth Innovation Promotion Association CAS (No. 2018446), and the New Star Project of Youth Science and Technology of Shaanxi Province in China (No. 2016KJXX-91). This work is part of the "Belt & Road" project of the Institute of Earth Environment, Chinese Academy of Sciences.

References

Cao, S., Li, C., & Yu, X. (2009). Impact of China's Grain for Green Project on the Landscape of Vulnerable Arid and Semi-Arid Agricultural Regions: A Case Study in Northern Shaanxi Province. *Journal of Applied Ecology, 46*(3), 536-543. doi:https://doi.org/10.1111/j.1365-2664.2008.01605.x

Cao, Z., Li, Y., Liu, Y., Chen, Y., & Wang, Y. (2018). When and where did the Loess Plateau turn "green"? Analysis of the tendency and breakpoints of the normalized difference vegetation index. *Land Degradation & Development, 29*(1), 162-175. doi:https://doi.org/10.1002/ldr.2852

Chen, B., Zhang, X., Tao, J., Wu, J., Wang, J., Shi, P., . . . Yu, C. (2014). The impact of climate change and anthropogenic activities on alpine grassland over the Qinghai-Tibet Plateau. *Agricultural and Forest Meteorology, 189-190*, 11-18. doi:https://doi.org/10.1016/j.agrformet.2014.01.002

Chen, C., Park, T., Wang, X., Piao, S., Xu, B., Chaturvedi, R. K., . . . Myneni, R. B. (2019). China and India lead in greening of the world through land-use management. *Nature Sustainability, 2*(2), 122-129. doi:https://doi.org/10.1038/s41893-019-0220-7

Chen, J., Ju, W., Ciais, P., Viovy, N., Liu, R., Liu, Y., & Lu, X. (2019). Vegetation structural change since 1981 significantly enhanced the terrestrial carbon sink. *Nature Communications, 10*, 7. doi:https://doi.org/10.1038/s41467-019-12257-8

Chen, Y., Wang, K., Lin, Y., Shi, W., Song, Y., & He, X. (2015). Balancing green and grain trade. *Nature Geoscience, 8*(10), 739-741. doi:https://doi.org/10.1038/ngeo2544

Dalal, R. C., Thornton, C. M., Allen, D. E., & Kopittke, P. M. (2021). A study over 33 years shows that carbon and nitrogen stocks in a subtropical soil are increasing under native vegetation in a changing climate. *Science of the Total Environment, 772*, 145019. doi:https://doi.org/10.1016/j.scitotenv.2021.145019

Davin, E. L., & de Noblet-Ducoudré, N. (2010). Climatic Impact of Global-Scale Deforestation: Radiative versus Nonradiative Processes. *Journal of Climate, 23*(1), 97-112. doi:https://doi.org/10.1175/2009jcli3102.1

Deng, L., Shangguan, Z., & Sweeney, S. (2014). "Grain for Green" driven land use change and carbon sequestration on the Loess Plateau, China. *Scientific Reports, 4*. doi:https://doi.org/10.1038/srep07039

Fasullo, J. (2012). A mechanism for land–ocean contrasts in global monsoon trends in a warming climate. *Climate Dynamics*. doi:https://doi.org/10.1007/s00382-011-1270-3

Feng, X., Fu, B., Piao, S., Wang, S., Ciais, P., Zeng, Z., . . . Wu, B. (2016). Revegetation in China's Loess Plateau is approaching sustainable water resource limits. *Nature Climate Change, 6*(11), 1019-1022. doi:https://doi.org/10.1038/nclimate3092

Gao, G., Ma, Y., & Fu, B. (2016). Temporal Variations of Flow-sediment Relationships in a Highly Erodible Catchment of the Loess Plateau, China. *Land Degradation & Development, 27*(3), 758-772. doi:https://doi.org/10.1002/ldr.2455

Grogan, K., Pflugmacher, D., Hostert, P., Verbesselt, J., & Fensholt, R. (2016). Mapping clearances in tropical dry forests using breakpoints, trend, and seasonal components from MODIS time series: does forest type matter? *Remote Sensing, 8*(8), 657. doi: https://doi.org/10.3390/rs8080657

Guo, L., Cheng, J., Luedeling, E., Koerner, S. E., He, J.-S., Xu, J., . . . Peng, C. (2017). Critical climate periods for grassland productivity on China's Loess Plateau. *Agricultural and Forest Meteorology, 233*, 101-109. doi:https://doi.org/10.1016/j.agrformet.2016.11.006

Hansen, M. C., Potapov, P. V., Moore, R., Hancher, M., Turubanova, S. A., Tyukavina, A., . . . Loveland, T. R. (2013). High-resolution global maps of 21st-century forest cover change. *Science, 342*(6160), 850-853. doi:https://doi.org/10.1126/science.1244693

Herrmann, S. M., Anyamba, A., & Tucker, C. J. (2005). Recent trends in vegetation dynamics in the African Sahel and their relationship to climate. *Global Environmental Change, 15*(4), 394-404. doi:https://doi.org/10.1016/j.gloenvcha.2005.08.004

Hu, C., Fu, B., Liu, G., Jin, T., & Guo, L. (2010). Vegetation patterns influence on soil microbial biomass and functional diversity in a hilly area of the Loess Plateau, China. *Journal of Soils and Sediments, 10*(6), 1082-1091. doi:https://doi.org/10.1007/s11368-010-0209-3

Huang, Y., Ren, H.-L., Chadwick, R., & Deng, Y. (2021). Decomposition of projected summer rainfall change over East Asia based on timeslice experiments. *Climate Dynamics*. doi:https://doi.org/10.1007/s00382-020-05602-x

Jia, X., Shao, M. a., Zhu, Y., & Luo, Y. (2017). Soil moisture decline due to afforestation across the Loess Plateau, China. *Journal of Hydrology, 546*, 113-122. doi:https://doi.org/10.1016/j.jhydrol.2017.01.011

Jiang, P., Liu, H., Piao, S., Ciais, P., Wu, X., Yin, Y., & Wang, H. (2019). Enhanced growth after extreme wetness compensates for post-drought carbon loss in dry forests. *Nature Communications, 10*(1), 195. doi:https://doi.org/10.1038/s41467-018-08229-z

Kisi, O., & Ay, M. (2014). Comparison of Mann–Kendall and innovative trend method for water quality parameters of the Kizilirmak River, Turkey. *Journal of Hydrology, 513*, 362-375. doi:https://doi.org/10.1016/j.jhydrol.2014.03.005

Lei, Y., Hoskins, B., & Slingo, J. (2014). Natural variability of summer rainfall over China in HadCM3. *Climate Dynamics, 42*(1), 417-432. doi:https://doi.org/10.1007/s00382-013-1726-8

Li, S., Liang, W., Fu, B., Lü, Y., Fu, S., Wang, S., & Su, H. (2016). Vegetation changes in recent large-scale ecological restoration projects and subsequent impact on water resources in China's Loess Plateau. *Science of the Total Environment, 569-570*, 1032-1039. doi:https://doi.org/10.1016/j.scitotenv.2016.06.141

Li, S., Yang, S., Liu, X., Liu, Y., & Shi, M. (2015). NDVI-Based Analysis on the Influence of Climate Change and Human Activities on Vegetation Restoration in the Shaanxi-Gansu-Ningxia Region, Central China. *Remote Sensing, 7*(9), 11163-11182. doi:https://doi.org/10.3390/rs70911163

Lian, X., Piao, S., Chen, A., Huntingford, C., Fu, B., Li, L. Z. X., . . . Roderick, M. L. (2021). Multifaceted characteristics of dryland aridity changes in a warming world. *Nature Reviews Earth & Environment*. doi:https://doi.org/10.1038/s43017-021-00144-0

Liu, Q., Wang, Y., Zhang, J., & Chen, Y. (2013). Filling Gullies to Create Farmland on the Loess Plateau. *Environmental Science & Technology, 47*(14), 7589-7590. doi:https://doi.org/10.1021/es402460r

Liu, Y., Cai, W., Sun, C., Song, H., Cobb, K. M., Li, J., . . . Linderholm, H. W. (2019). Anthropogenic Aerosols Cause Recent Pronounced Weakening of Asian Summer Monsoon Relative to Last Four Centuries. *Geophysical Research Letters, 46*(10), 5469-5479. doi:https://doi.org/10.1029/2019GL082497

Liu, Y., Stanturf, J., & Lu, H. (2008). Modeling the Potential of the Northern China Forest Shelterbelt in Improving Hydroclimate Conditions1. *JAWRA Journal of the American Water Resources Association, 44*(5), 1176-1192. doi:https://doi.org/10.1111/j.1752-1688.2008.00240.x

Liu, Z., Wang, J., Wang, X., & Wang, Y. (2020). Understanding the impacts of 'Grain for Green' land management practice on land greening dynamics over the Loess Plateau of China. *Land Use Policy, 99*, 5084-5084. doi:https://doi.org/10.1016/j.landusepol.2020.105084

Los, S. O. (2013). Analysis of trends in fused AVHRR and MODIS NDVI data for 1982–2006: Indication for a CO2 fertilization effect in global vegetation. *Global Biogeochemical Cycles, 27*(2), 318-330. doi:https://doi.org/10.1002/gbc.20027

Lü, Y., Fu, B., Feng, X., Zeng, Y., Liu, Y., Chang, R., . . . Wu, B. (2012). A Policy-Driven Large Scale Ecological Restoration: Quantifying Ecosystem Services Changes in the Loess Plateau of China. *PLoS One, 7*(2), e31782. doi:https://doi.org/10.1371/journal.pone.0031782

McVicar, T. R., Li, L., Van Niel, T. G., Zhang, L., Li, R., Yang, Q., . . . Gao, P. (2007). Developing a decision support tool for China's re-vegetation program: Simulating regional impacts of afforestation on average annual streamflow in the Loess Plateau. *Forest Ecology and Management, 251*(1), 65-81. doi:https://doi.org/10.1016/j.foreco.2007.06.025

McVicar, T. R., Van Niel, T. G., Li, L., Wen, Z., Yang, Q., Li, R., & Jiao, F. (2010). Parsimoniously modelling perennial vegetation suitability and identifying priority areas to support China's re-vegetation program in the Loess Plateau: Matching model complexity to data availability. *Forest Ecology and Management, 259*(7), 1277-1290. doi:https://doi.org/10.1016/j.foreco.2009.05.002

Mendoza-Ponce, A., Corona-Nunez, R., Kraxner, F., Leduc, S., & Patrizio, P. (2018). Identifying effects of land use cover changes and climate change on terrestrial ecosystems and carbon stocks in Mexico. *Global Environmental Change-Human and Policy Dimensions, 53*, 12-23. doi:https://doi.org/10.1016/j.gloenvcha.2018.08.004

Myneni, R. B., Keeling, C. D., Tucker, C. J., Asrar, G., & Nemani, R. R. (1997). Increased plant growth in the northern high latitudes from 1981 to 1991. *Nature, 386*(6626), 698-702. doi:https://doi.org/10.1038/386698a0

Peng, S., Piao, S., Zeng, Z., Ciais, P., Zhou, L., Li, L. Z. X., . . . Zeng, H. (2014). Afforestation in China cools local land surface temperature. *Proceedings of the National Academy of Sciences, 111*(8), 2915-2919. doi:https://doi.org/10.1073/pnas.1315126111

Piao, S., Fang, J., & He, J. (2006). Variations in vegetation net primary production in the Qinghai-Xizang Plateau, China, from 1982 to 1999. *Climatic Change, 74*(1-3), 253-267. doi:https://doi.org/10.1007/s10584-005-6339-8

Piao, S., Wang, X., Park, T., Chen, C., Lian, X., He, Y., . . . Myneni, R. B. (2020). Characteristics, drivers and feedbacks of global greening. *Nature Reviews Earth and Environment, 1*(1), 14-27. doi:https://doi.org/10.1038/s43017-019-0001-x

Piao, S., Yin, G., Tan, J., Cheng, L., Huang, M., Li, Y., . . . Peng, S. (2015). Detection and attribution of vegetation greening trend in China over the last 30years. *Global Change Biology, 21*(4), 1601-1609. doi:https://doi.org/10.1111/gcb.12795

Sicard, P., Mangin, A., Hebel, P., & Malléa, P. (2010). Detection and estimation trends linked to air quality and mortality on French Riviera over the 1990–2005 period. *Science of the Total Environment, 408*(8), 1943-1950. doi:https://doi.org/10.1016/j.scitotenv.2010.01.024

Song, F., Zhou, T., & Qian, Y. (2014). Responses of East Asian summer monsoon to natural and anthropogenic forcings in the 17 latest CMIP5 models. *Geophysical Research Letters, 41*(2), 596-603. doi:https://doi.org/10.1002/2013GL058705

Song, Y., Jin, L., & Wang, H. (2018). Vegetation changes along the Qinghai-Tibet Plateau engineering corridor since 2000 induced by climate change and human activities. *Remote Sensing, 10*(1), 95. doi:https://doi.org/10.3390/rs10010095

Stow, D., Daeschner, S., Hope, A., Douglas, D., Petersen, A., Myneni, R., . . . Oechel, W. (2003). Variability of the Seasonally Integrated Normalized Difference Vegetation Index Across the North Slope of Alaska in the 1990s. *International Journal of Remote Sensing, 24*(5), 1111-1117. doi:https://doi.org/10.1080/0143116021000020144

Sun, W., Song, X., Mu, X., Gao, P., Wang, F., & Zhao, G. (2015). Spatiotemporal vegetation cover variations associated with climate change and ecological restoration in the Loess Plateau. *Agricultural and Forest Meteorology, 209-210*, 87-99. doi:https://doi.org/10.1016/j.agrformet.2015.05.002

Wang, H., Liu, G.-h., Li, Z.-s., Ye, X., Wang, M., & Gong, L. (2016). Driving force and changing trends of vegetation phenology in the Loess Plateau of China from 2000 to 2010. *Journal of Mountain Science, 13*(5), 844-856. doi:https://doi.org/10.1007/s11629-015-3465-2

Wang, H., Lu, H., Zhao, L., Zhang, H., Lei, F., & Wang, Y. (2019). Asian monsoon rainfall variation during the Pliocene forced by global temperature change. *Nature Communications, 10*. doi:https://doi.org/10.1038/s41467-019-13338-4

Wang, H., Yang, Z., Saito, Y., Liu, J. P., Sun, X., & Wang, Y. (2007). Stepwise decreases of the Huanghe (Yellow River) sediment load (1950–2005): Impacts of climate change and human activities. *Global and Planetary Change, 57*(3-4), 331-354. doi:https://doi.org/10.1016/j.gloplacha.2007.01.003

Wang, S., Fu, B., Piao, S., Lü, Y., Ciais, P., Feng, X., & Wang, Y. (2016). Reduced sediment transport in the Yellow River due to anthropogenic changes. *Nature Geoscience, 9*(1), 38-41. doi:https://doi.org/10.1038/ngeo2602

Wang, S., Fu, B. J., Gao, G. Y., Yao, X. L., & Zhou, J. (2012). Soil moisture and evapotranspiration of different land cover types in the Loess Plateau, China. *Hydrology and Earth System Sciences, 16*(8), 2883-2892. doi:https://doi.org/10.5194/hess-16-2883-2012

Wang, X., Piao, S., Ciais, P., Friedlingstein, P., Myneni, R. B., Cox, P., . . . Chen, A. (2014). A two-fold increase of carbon cycle sensitivity to tropical temperature variations. *Nature, 506*(7487), 212-215. doi:https://doi.org/10.1038/nature12915

Wang, Y., Brandt, M., Zhao, M., Tong, X., Xing, K., Xue, F., . . . Fensholt, R. (2018). Major forest increase on the Loess Plateau, China (2001–2016). *Land Degradation & Development, 29*(11), 4080-4091. doi:https://doi.org/10.1002/ldr.3174

Wang, Y., Fu, B., Chen, L., Lu, Y., & Gao, Y. (2011). Check Dam in the Loess Plateau of China: Engineering for Environmental Services and Food Security. *Environmental Science & Technology, 45*(24), p.10298-10299. doi:https://doi.org/10.1021/es2038992

Wang, Y., Shao, M. a., Zhu, Y., Sun, H., & Fang, L. (2018). A new index to quantify dried soil layers in water-limited ecosystems: A case study on the Chinese Loess Plateau. *Geoderma, 322*, 1-11. doi:https://doi.org/10.1016/j.geoderma.2018.02.007

Wang, Y., & Yao, S. (2019). Effects of restoration practices on controlling soil and water losses in the Wei River Catchment, China: An estimation based on longitudinal field observations. *Forest Policy and Economics, 100*, 120-128. doi:https://doi.org/10.1016/j.forpol.2018.12.001

Xiao, J. (2014). Satellite evidence for significant biophysical consequences of the “Grain for Green” Program on the Loess Plateau in China. *Journal of Geophysical Research: Biogeosciences, 119*(12), 2261-2275. doi:https://doi.org/10.1002/2014JG002820

Xie, S., Mo, X., Hu, S., & Liu, S. (2020). Contributions of climate change, elevated atmospheric CO2 and human activities to ET and GPP trends in the Three-North Region of China. *Agricultural and Forest Meteorology, 295*. doi:https://doi.org/10.1016/j.agrformet.2020.108183

Xin, Z., Xu, J., & Zheng, W. (2008). Spatiotemporal variations of vegetation cover on the Chinese Loess Plateau (1981–2006): Impacts of climate changes and human activities. *Science in China Series D: Earth Sciences, 51*(1), 67-78. doi:https://doi.org/10.1007/s11430-007-0137-2

Xu, K., Zhu, C., & Wang, W. (2016). The cooperative impacts of the El Nino-Southern Oscillation and the Indian Ocean Dipole on the interannual variability of autumn rainfall in China. *International Journal of Climatology, 36*(4), 1987-1999. doi:https://doi.org/10.1002/joc.4475

Xu, L., Myneni, R., Chapin Iii, F., Callaghan, T. V., Pinzon, J., Tucker, C. J., . . . Tømmervik, H. (2013). Temperature and vegetation seasonality diminishment over northern lands. *Nature Climate Change, 3*(6), 581-586. doi:https://doi.org/10.1038/nclimate1836

Yang, H., Kang, W., Yu, Y., Yin, X., Wang, P., & Zhang, X. (2017). A new approach to evaluate the particle growth and sedimentation of dispersed polymer microsphere profile control system based on multiple light scattering. *Powder Technology, 315*, 477-485. doi:https://doi.org/10.1016/j.powtec.2017.04.001

Zhang, B., He, C., Burnham, M., & Zhang, L. (2016). Evaluating the coupling effects of climate aridity and vegetation restoration on soil erosion over the Loess Plateau in China. *Science of the Total Environment, 539*, 436-449. doi:https://doi.org/10.1016/j.scitotenv.2015.08.132

Zhang, C., Zhao, C., Yu, Z., Zhang, H., Zhou, A., Zhang, X., . . . Shen, J. (2020). Western Pacific Ocean influences on monsoon precipitation in the southwestern Chinese Loess Plateau since the mid-Holocene. *Climate Dynamics, 54*(5-6), 3121-3134. doi:https://doi.org/10.1007/s00382-020-05159-9

Zhang, W., Brandt, M., Penuelas, J., Guichard, F., Tong, X., Tian, F., & Fensholt, R. (2019). Ecosystem structural changes controlled by altered rainfall climatology in tropical savannas. *Nature Communications, 10*, 7. doi:https://doi.org/10.1038/s41467-019-08602-6

Zhang, Y., Yu, G., Yang, J., Wimberly, M. C., Zhang, X., Tao, j., . . . Zhu, J. (2014). Climate-driven global changes in carbon use efficiency. *Global Ecology and Biogeography, 23*(2), 144-155. doi:https://doi.org/10.1111/geb.12086

Zheng, K., Wei, J.-Z., Pei, J.-Y., Cheng, H., Zhang, X.-L., Huang, F.-Q., . . . Ye, J.-S. (2019). Impacts of climate change and human activities on grassland vegetation variation in the Chinese Loess Plateau. *Science of the Total Environment, 660*, 236-244. doi:https://doi.org/10.1016/j.scitotenv.2019.01.022

Zhu, Z., Piao, S., Myneni, R. B., Huang, M., Zeng, Z., Canadell, J. G., . . . Zeng, N. (2016). Greening of the Earth and its drivers. *Nature Climate Change, 6*(8), 791-795. doi:https://doi.org/10.1038/nclimate3004

Fig. 1. Quadrats locations in the Loess Plateau of China. “NMS” indicates a national meteorological station

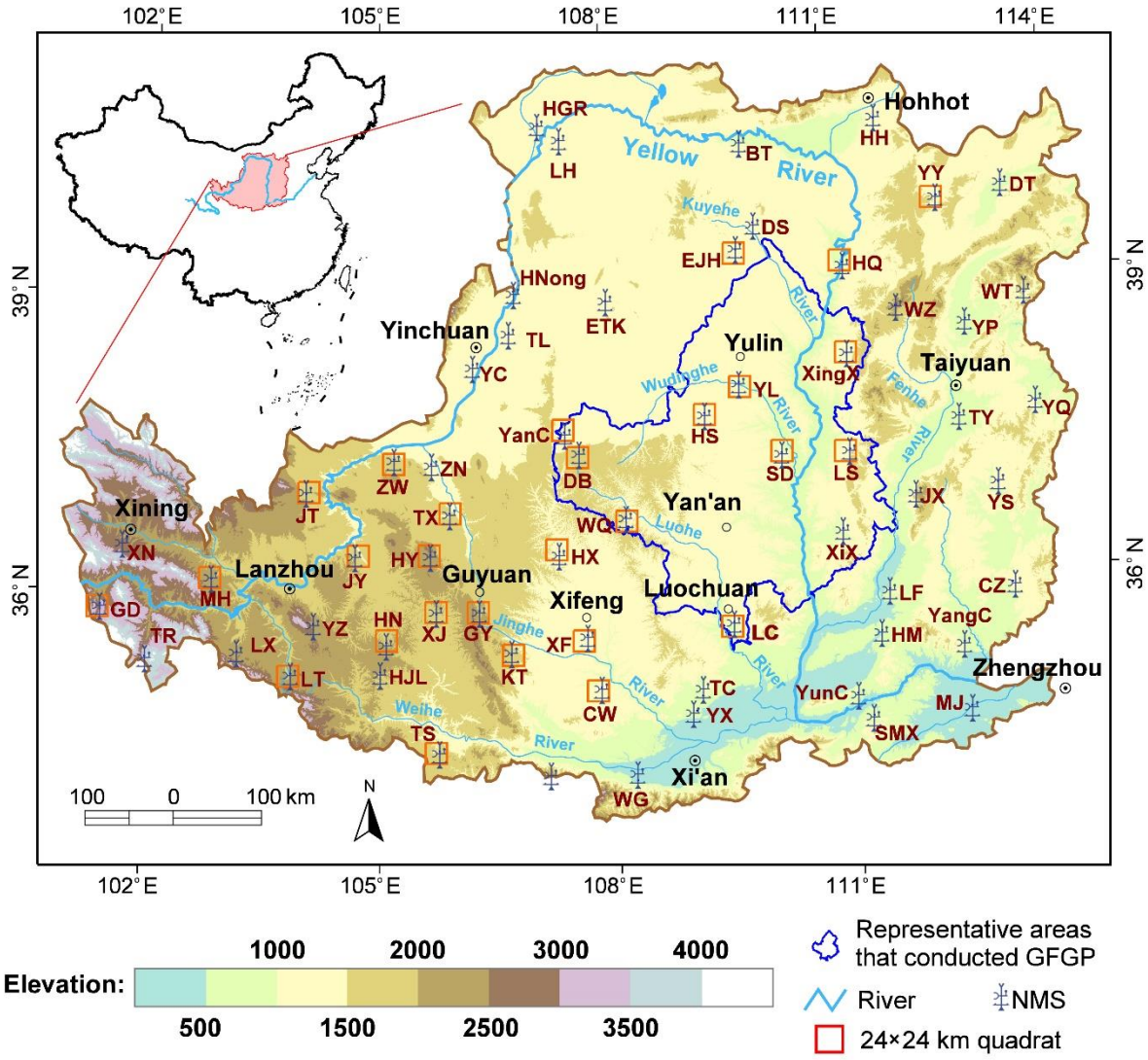
102°E
105°E
108°E
111°E
114°E
39°N
36°N
Hohhot
HGR
HH
LH
Yellow
River
BT
YY
DT
Kuyehe
DS
EJH
HQ
HNong
WT
WZ
YP
Yinchuan
TL
ETK
Yulin
Taiyuan
YC
XingX
Wuding
he
River
YL
Fenhe
River
TY
YQ
YanC
HS
SD
LS
ZW
ZN
DB
Yan'an
JX
YS
Xining
JT
TX
WQ
Luohe
XiX
XN
HY
HX
Lanzhou
JY
Guyuan
Luochuan
LF
CZ
MH
Xifeng
YangC
GD
HN
XJ
GY
Jinghe
XF
LC
HM
TR
YZ
LX
River
Zhengzhou
LT
HJL
KT
TC
YunC
MJ
Weihe
CW
YX
River
River
SMX
TS
Xi'an
WG
100
0
100 km
N
Elevation:
1000
2000
3000
4000
500
1500
2500
3500
Representative areas that conducted GFGP
River
NMS
24×24 km quadrat

Fig. 2. Schematic diagram of the double mass curve (DMC) method. The DMCs were generated using the two cumulative variables of CSINDVI (CCSINDVI) and CI (CCI) from 1982 to the specific year when the CSINDVI and CI were generated.

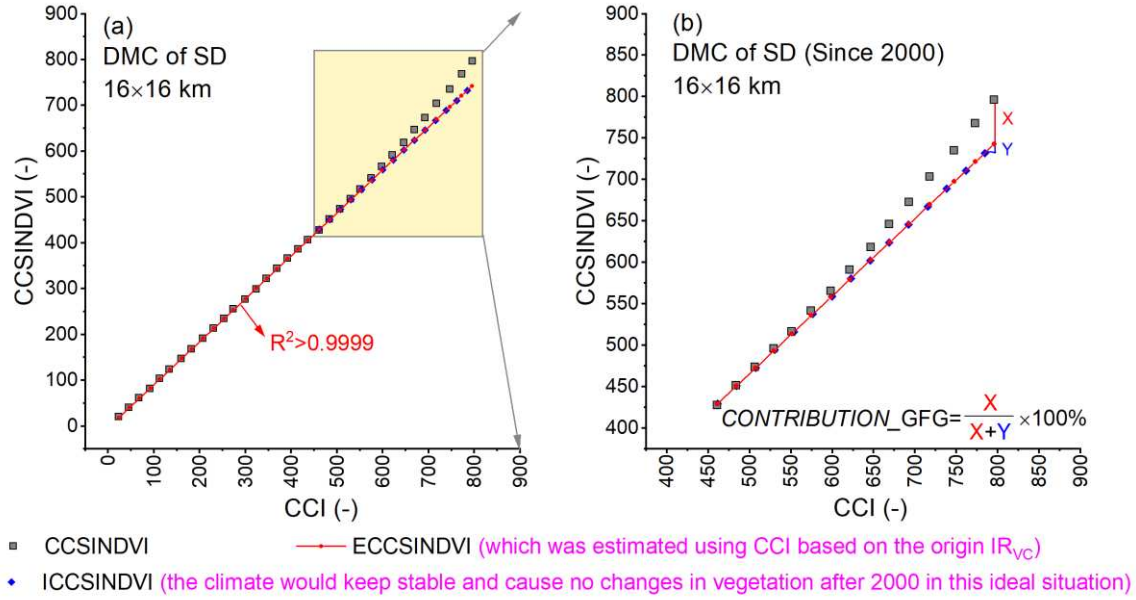

Fig. 3. Significance of the changes in SINDVI over 38 years: (a) 1982 to 2000 and (b) 2001-2019. The green and purple colours indicate the confidence level (α was set to 0.005, 0.01, 0.05 or 0.1) of increases and decreases in SINDVI, respectively, with darker colours indicating greater changes. The white colour indicates non-significant changes in SINDVI at a confidence level of 0.1.

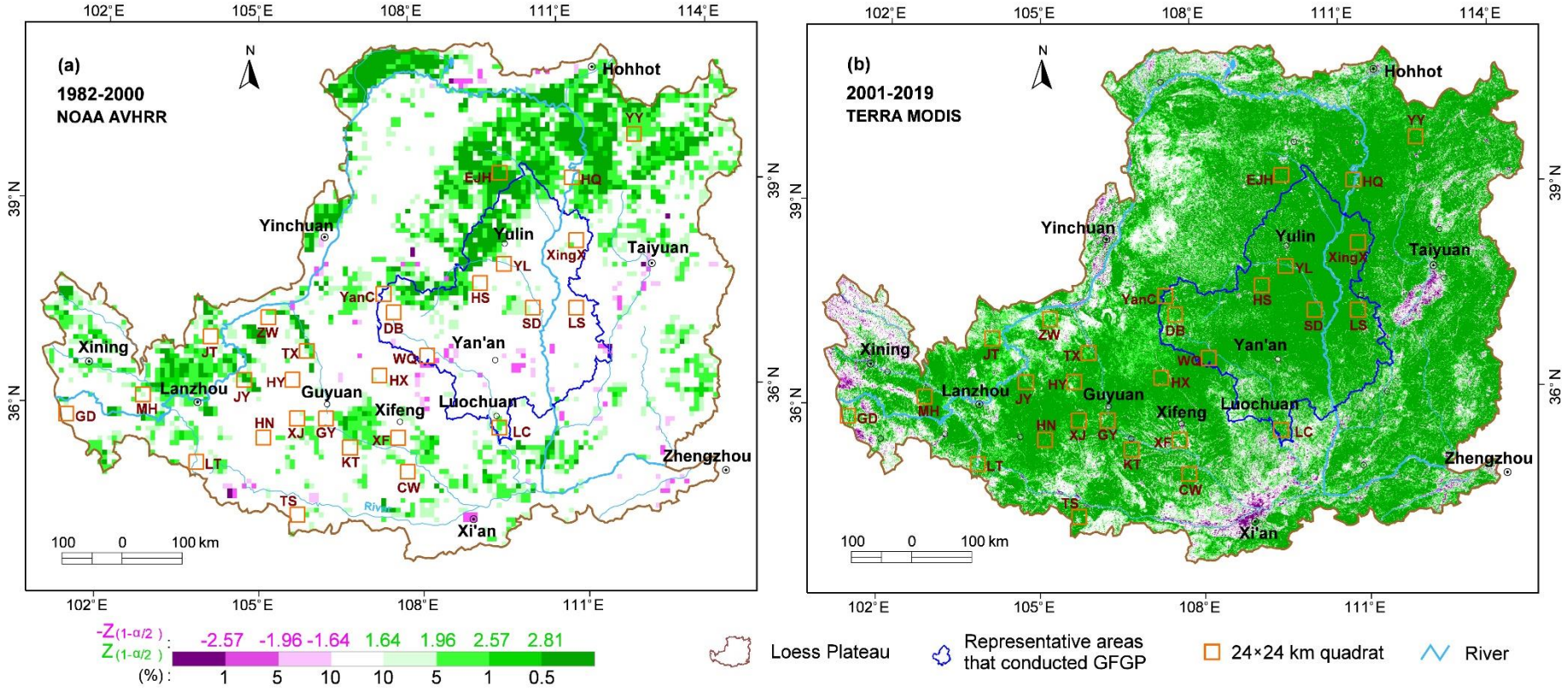

Fig. 4 Relationship between annual precipitation (*P*), annual average temperature (*T*) and annually maximal vegetation coverage (VC_{max}) in the representative areas that conducted GFGP. The VC_{max} was calculated as: $VC_{max} = \left(\frac{NDVI_{max}-0.1}{0.8-0.1}\right)^2$, where the $NDVI_{mas}$ was the maximum of NDVI values (AVHRR GIMMS NDVI) during one year.

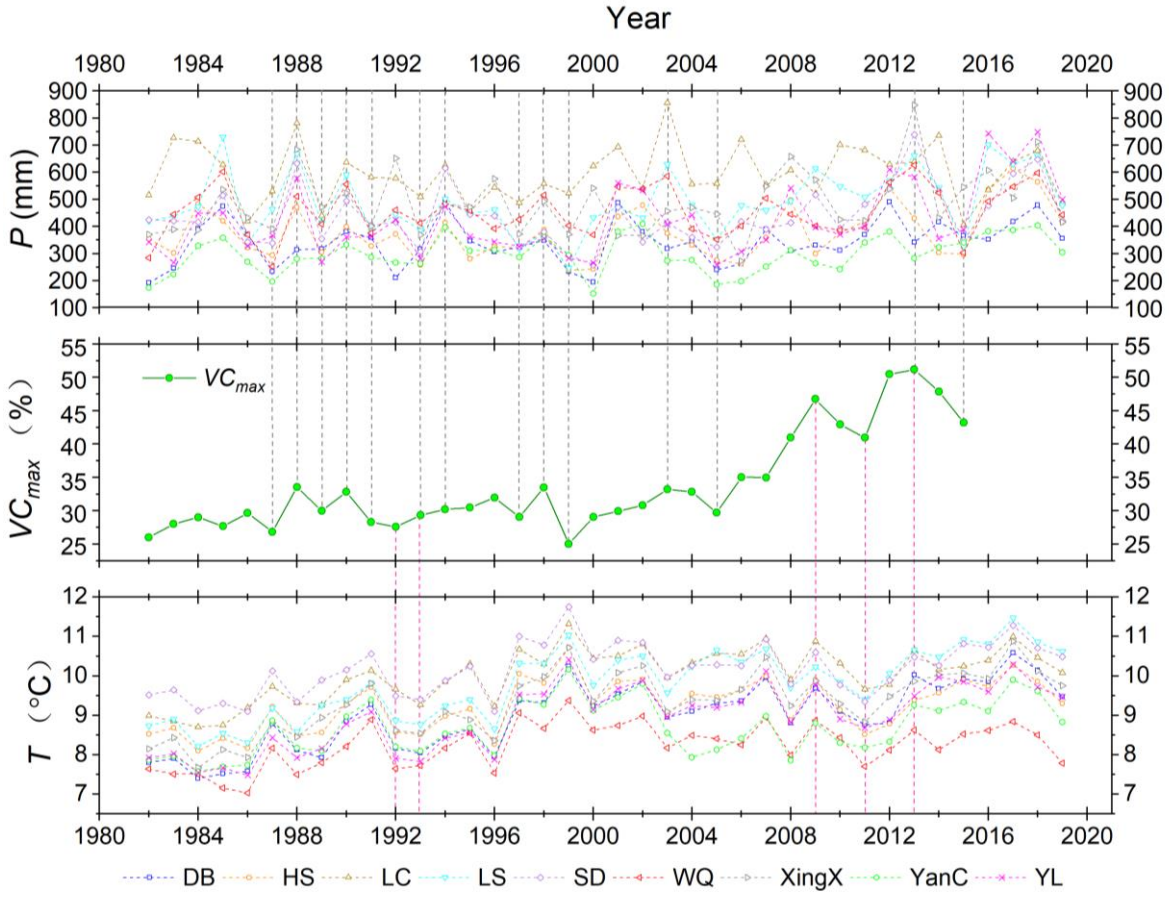

Fig. 5. *CONTRIBUTION*_GFGP in 28 quadrats at a 24 × 24 km scale till 2015.

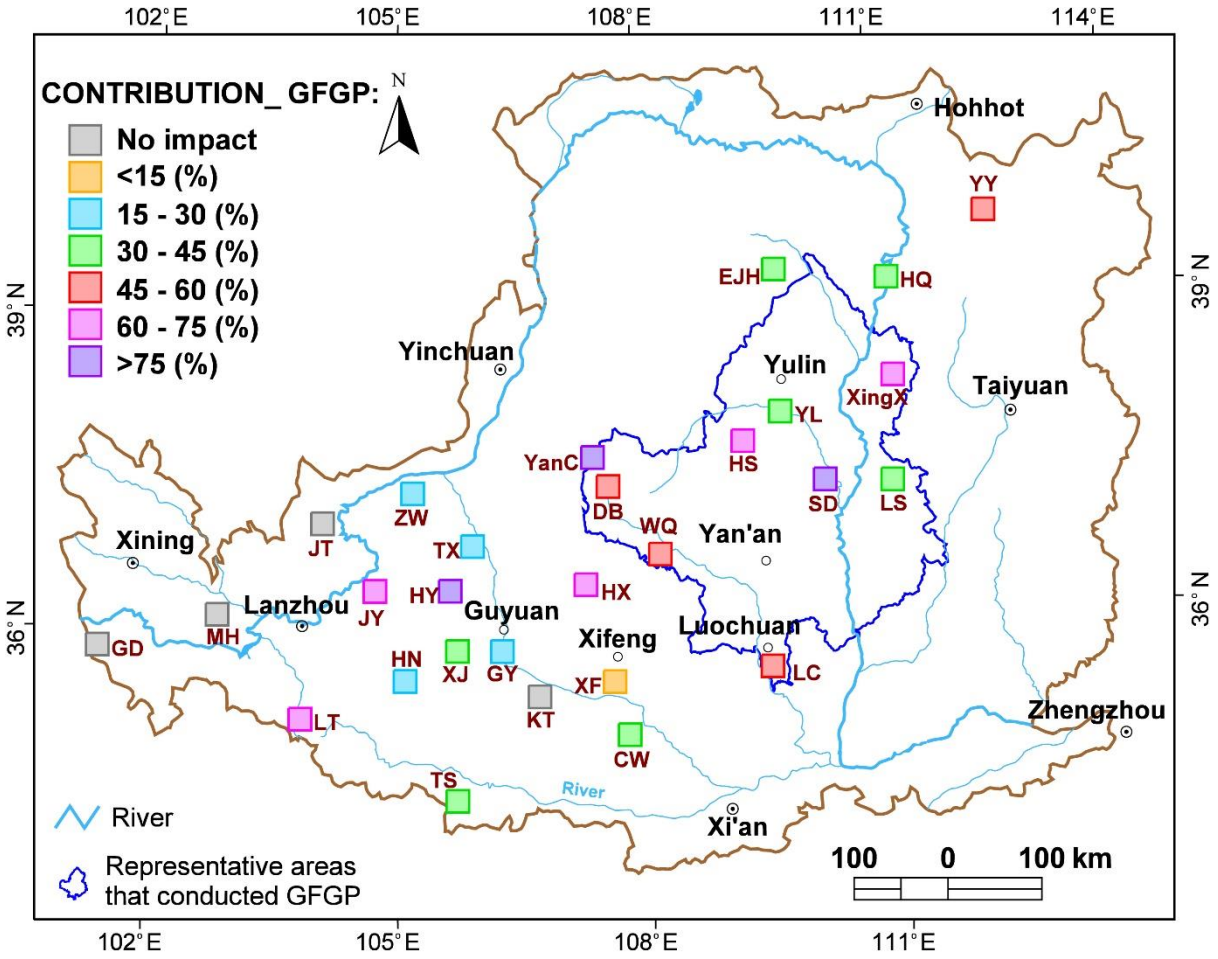

Fig. 6. Temporal variation of *CONTRIBUTION*_GFGP in the 9 quadrats within the representative area that conducted GFG project at a 24 × 24 km scale from 2002 to 2015.

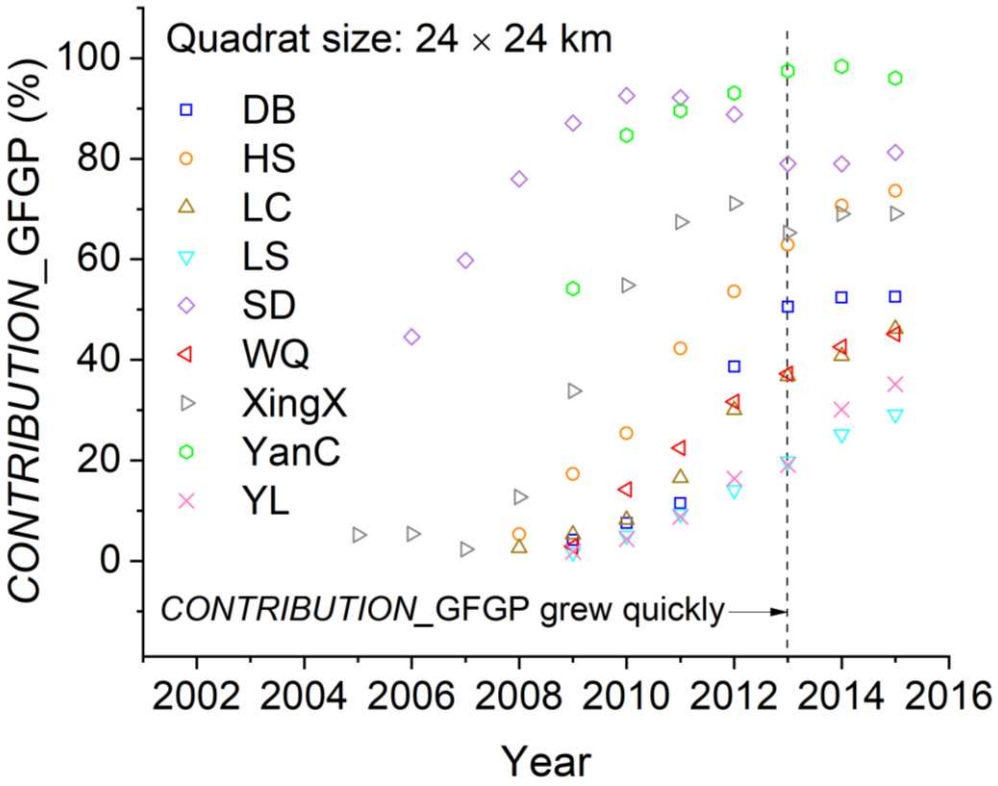

Fig. 7. Significance of the changes in P (Sig_P) and T (Sig_T): (a) Sig_P and (b) Sig_T from 1982 to 1999; (c) Sig_P and (d) Sig_T from 1999 to 2019. The confidence level (α) was set to 0.005, 0.01, 0.05 or 0.1, respectively, with darker colours and bigger size indicating greater changes. The "NS" indicates non-significant changes at a confidence level of 0.1.

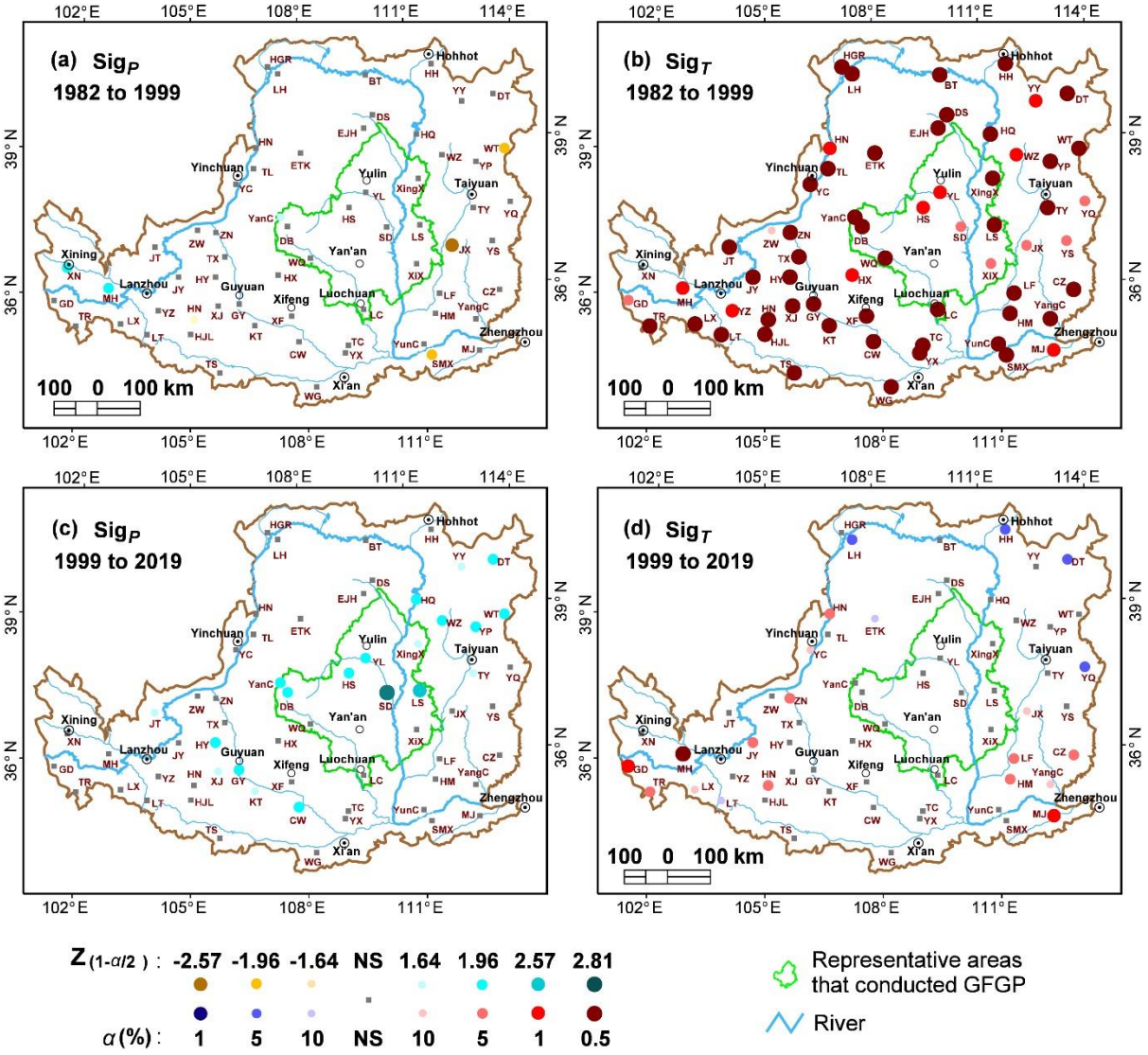

Supplementary Information

Quantitative contribution of the Grain for Green project to vegetation greening and its spatiotemporal variation across the Chinese Loess Plateau

Yi Song[1, 2], Yunqiang Wang[1, 2 *], Long Jin[3], Weiyu Shi[4], Jagannath Aryal[5], Alexis Comber[6]

[1] State Key Laboratory of Loess and Quaternary Geology, Institute of Earth Environment, Chinese Academy of Sciences, Xi'an 710061, China

[2] CAS Center for Excellence in Quaternary Science and Global Change, Xi'an, 710061, China

[3] College of Civil Engineering, Xi'an University of Science and Technology, Xi'an 710065, China

[4] School of Geographical Sciences, Southwest University, Chongqing 400715, China

[5] Faculty of Engineering and IT, Department of Infrastructure Engineering, University of Melbourne, Parkville, Victoria, Australia

[6] School of Geography, University of Leeds, Leeds, LS2 9JT, United Kingdom

* Corresponding author, E-mail address: wangyq@ieecas.cn (Y. Wang)

Fig. S1. Comparison between CSINDVI and mean SINDVI both of which were calculated using AVHRR NDVI dataset within a 24×24 km quadrate in Ejin Horo Banner (EJH) from 1982 to 2015. The vegetation coverage in this quadrate was about 15.6% in 2000.

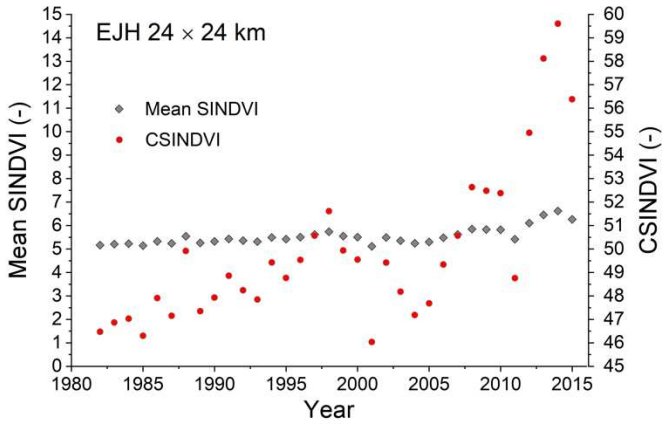

Fig. S2. Significance of the changes in SINDVI over 15 years (2001-2015) calculated using (a) AVHRR GIMMS NDVI and (b) MODIS NDVI, respectively. The green and purple colours indicate the confidence level (α was set to 0.005, 0.01, 0.05 or 0.1) of increases and decreases in SINDVI, respectively, with darker colours indicating greater changes. The white colour indicates non-significant changes in SINDVI at a confidence level of 0.1.

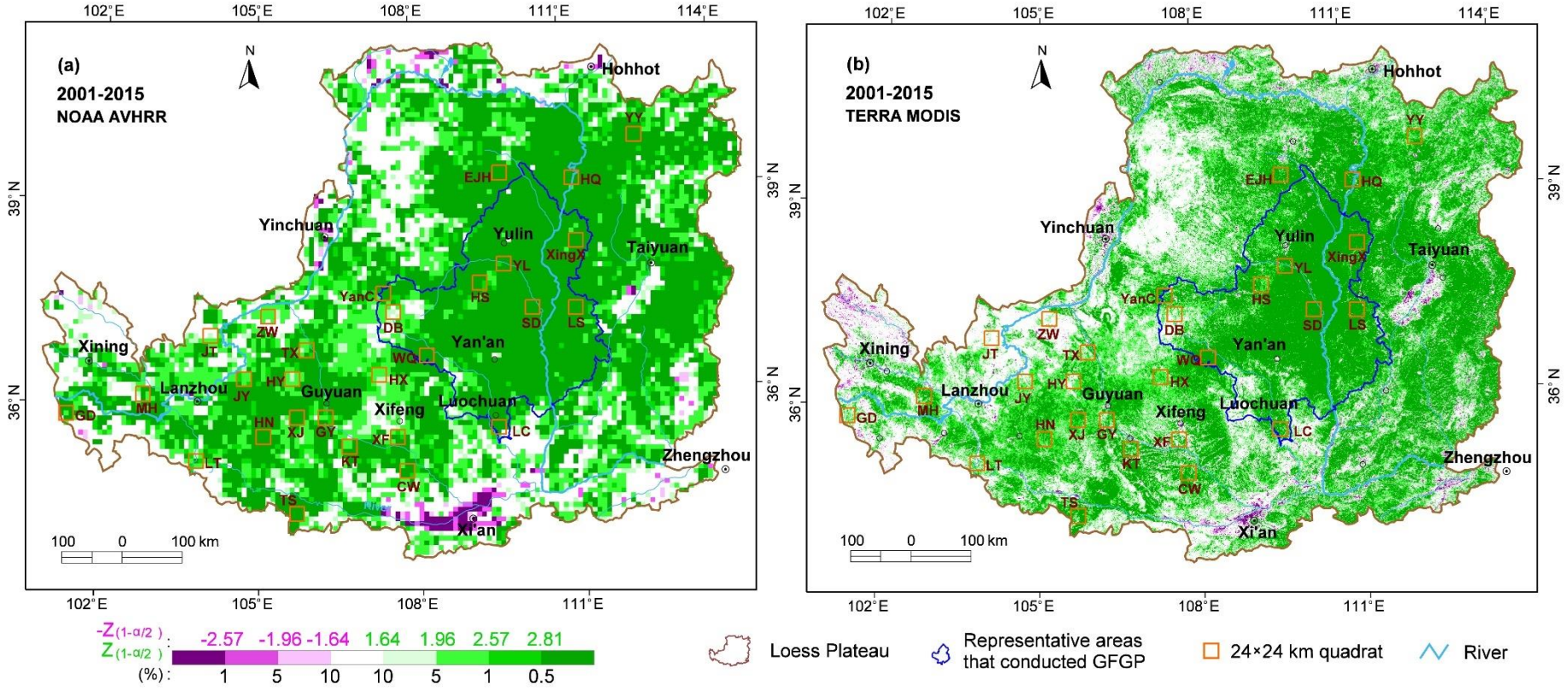

Fig. S3. Annual maximal vegetation coverage (VC_{max}) from 2000 to 2019. VC_{max} was calculated as: $VC_{max} = \left(\frac{NDVI_{max}-0.1}{0.8-0.1}\right)^2$, where the $NDVI_{mas}$ was the maximum of NDVI values (MODIS NDVI) during one year.

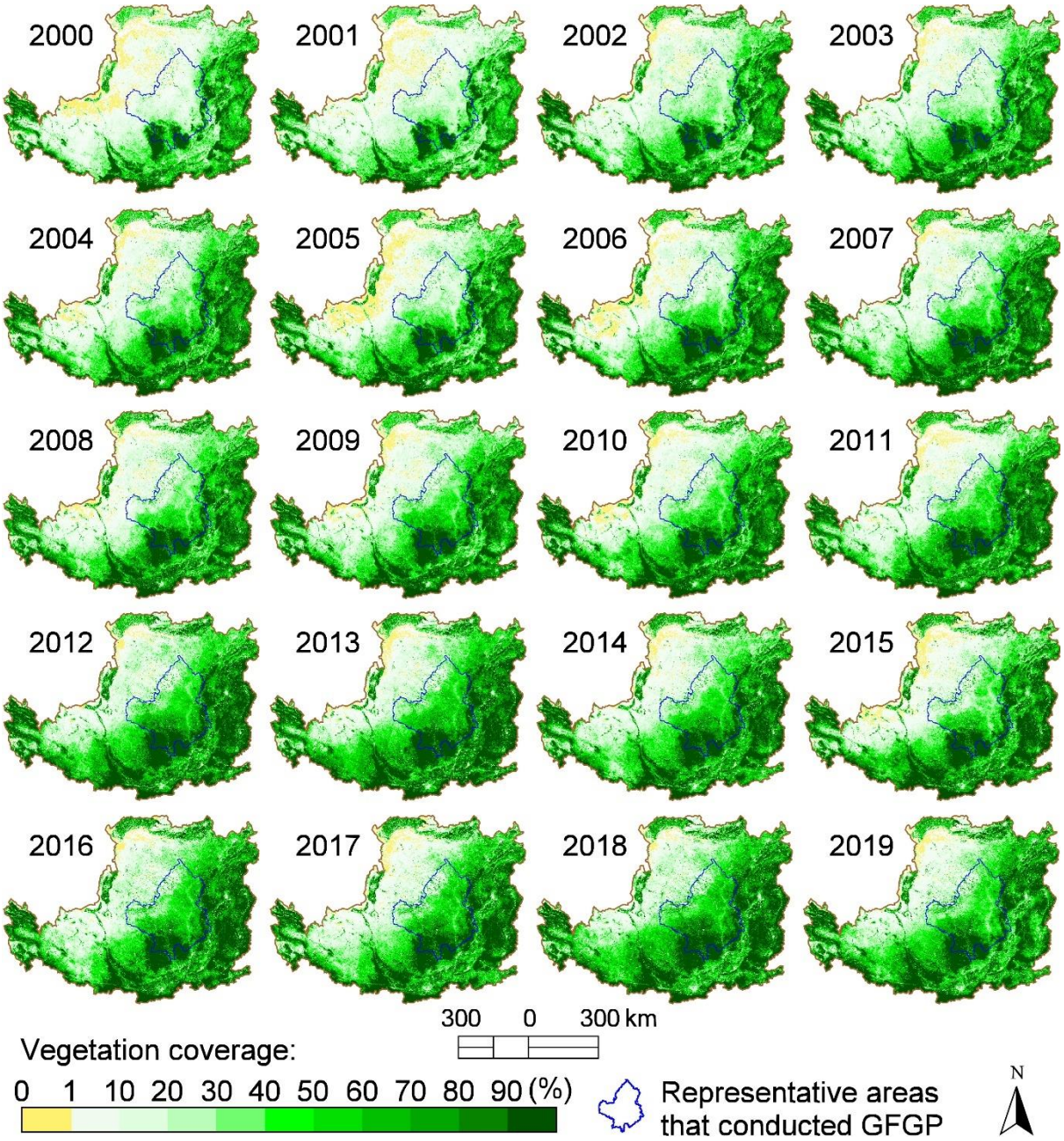

Fig. S4. SINDVIs derived from the AVHRR GIMMS NDVI and MODIS MOD13Q1 NDVI datasets and climate observations (*P* and *T*) at the 28 NMSs.

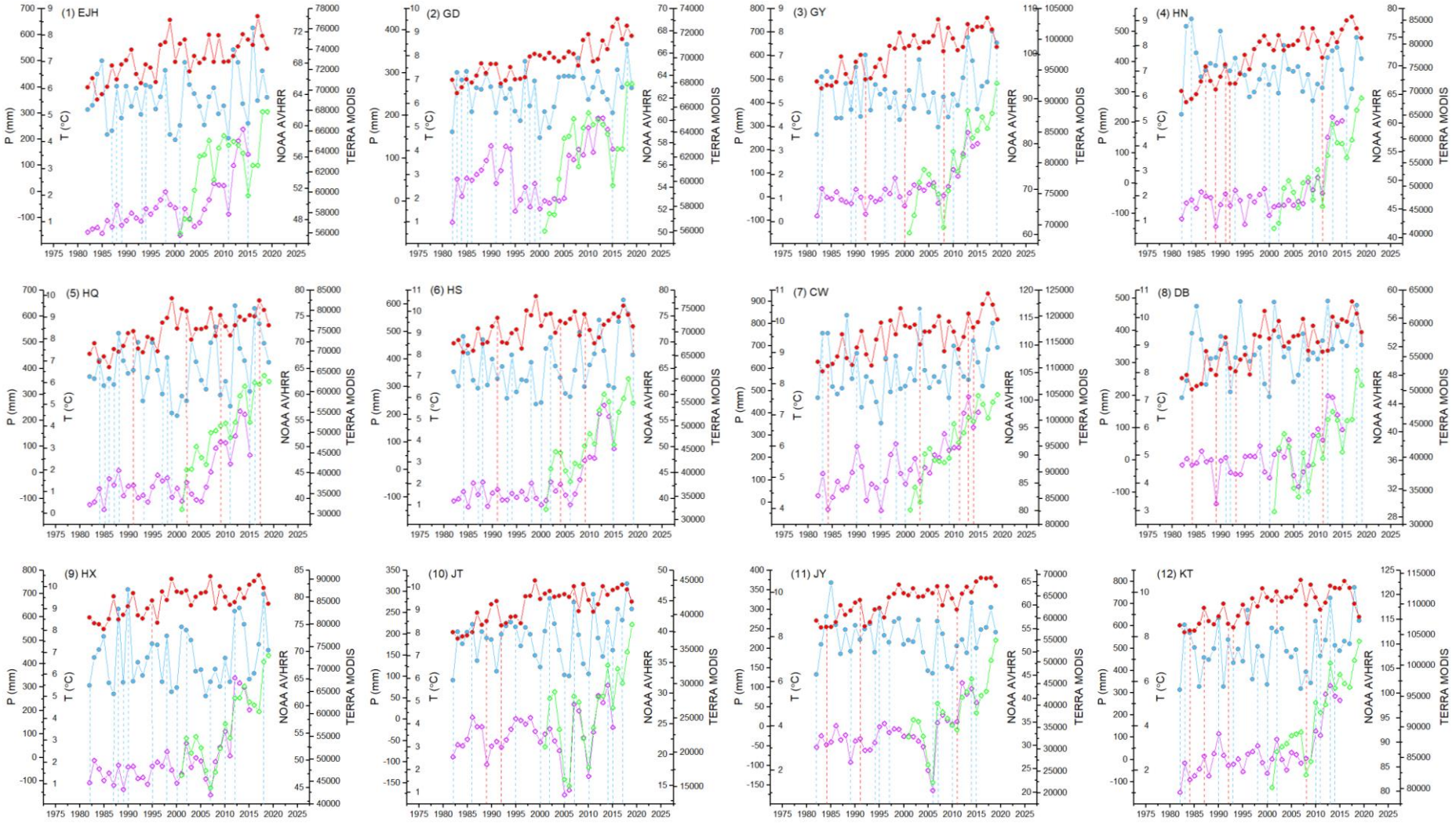

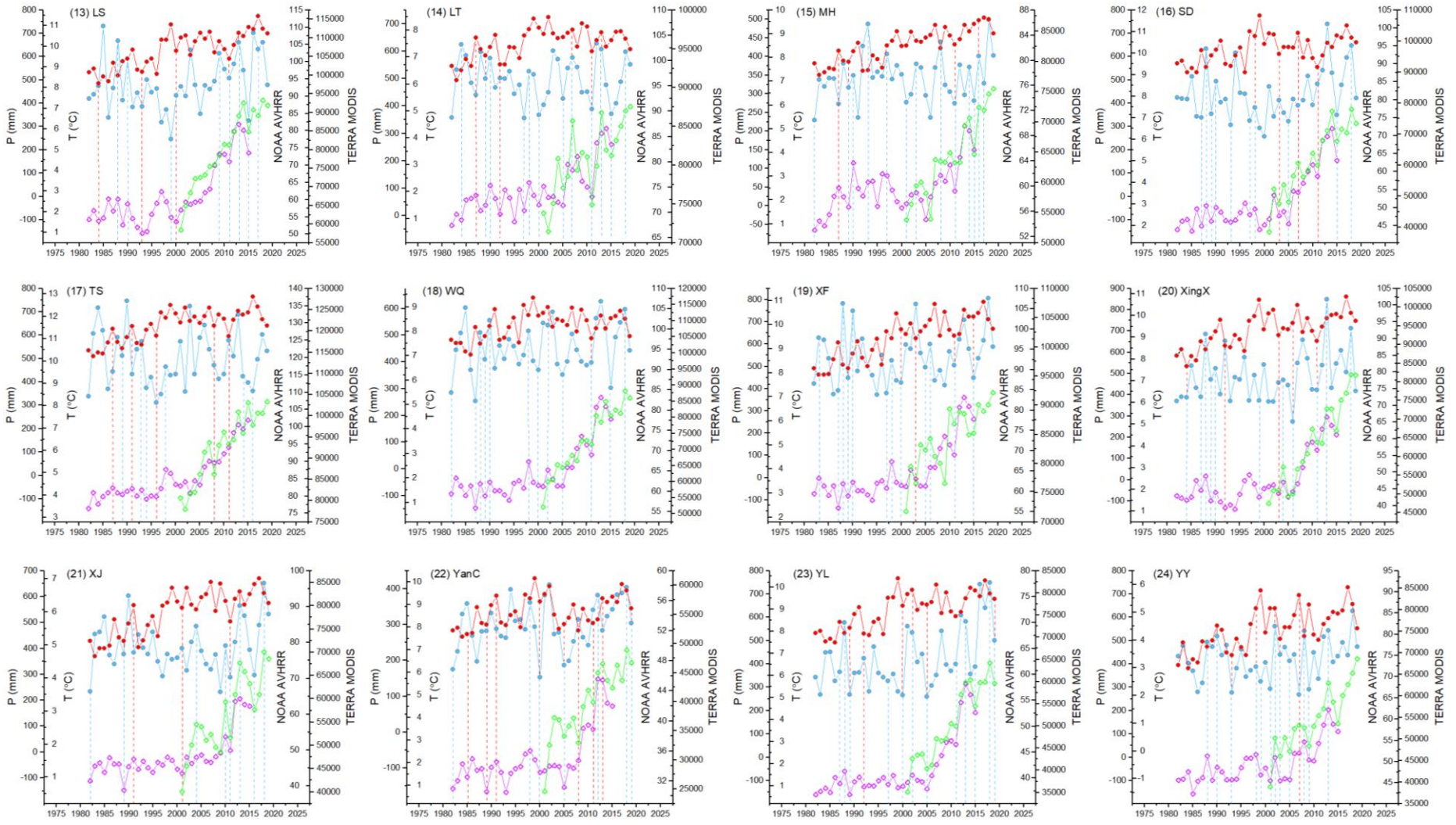
(13) LS
(14) LT
(15) MH
(16) SD
(17) TS
(18) WQ
(19) XF
(20) XingX
(21) XJ
(22) YanC
(23) YL
(24) YY
P (mm)
T (°C)
NOAA AVHRR
TERRA MODIS

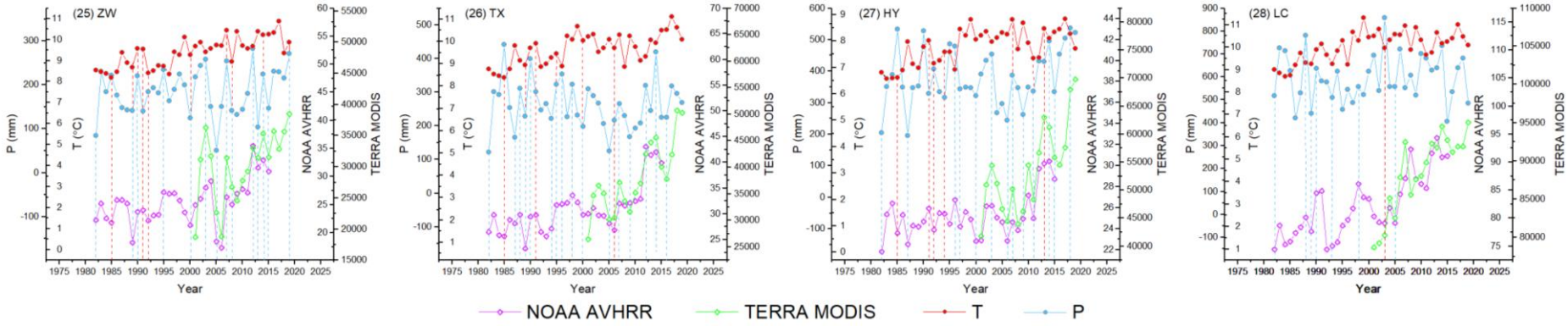
(25) ZW
(26) TX
(27) HY
(28) LC
P (mm)
T (°C)
NOAA AVHRR
TERRA MODIS
Year
NOAA AVHRR
TERRA MODIS
T
P

Table S1. National meteorological stations which used in this study.

Province	ID	Name	Short name	Longitude	lantitude
Qinghai	1	Guide	GD	101°25.2′	35°51.5′
	2	Minhe	MH	102°50.5′	36°8.4′
	3	Tongren	TR	102°0.3′	35°20.7′
	4	Xining	XN	101°44.3′	36°32.2′
Gansu	5	Linxia	LX	103°10.6′	35°24.6′
	6	Lintao	LT	103°51.7′	35°11.7′
	7	Huining	HN	105°5.0′	35°30.6′
	8	Kongtong	KT	106°40.4′	35°22.7′
	9	Xifeng	XF	107°38.6′	35°33.6′
	10	Yuzhong	YZ	104°8.9′	35°41.7′
	11	Huajialing	HJL	105°0.0′	35°12.7′
	12	Tianshui	TS	105°45.2′	34°25.0′
	13	Huanxian	HX	107°18.5′	36°24.3′
	14	Jingtai	JT	104°2.8′	37°0.1′
	15	Jingyuan	JY	104°40.9′	36°23.3′
Inner Mongolia	16	Baotou	BT	109°52.1′	40°27.7′
	17	Hohhot	HH	111°42.5′	40°36.7′
	18	Etuoke Banner	ETK	107°59.7′	38°54.3′
	19	Ejin Horo Banner	EJH	109°45.1′	39°22.2′
	20	Hangjing Rear Banner	HGR	107°8.5′	40°41.6′
	21	Dongsheng	DS	110°0.1′	39°38.1′
	22	Linhe	LH	107°25.5′	40°32.7′
Ningxia	23	Zhongning	ZN	105°40.2′	37°18.0′

	24	Haiyuan	HY	105°39.1′	36°23.3′
	25	Guyuan	GY	106°16.3′	35°49.5′
	26	Yinchuan	YC	106°13.3′	38°17.6′
	27	Zhongwei	ZW	105°11.0′	37°20.9′
	28	Tongxin	TX	105°54.2′	36°48.1′
	29	Taole	TL	106°42.4′	38°36.5′
	30	Huinong	HNong	106°46.4′	39°1.3′
	31	Xiji	XJ	105°43.2′	35°47.5′
	32	Yulin	YL	109°43.1′	38°2.7′
	33	Yanchi	YanC	107°24.5′	37°35.8′
	34	Dingbian	DB	107°35.6′	37°23.9′
	35	Wuqi	WQ	108°10.7′	36°44.2′
	36	Hengshan	HS	109°15.0′	37°44.8′
Shaanxi	37	Suide	SD	110°14.2′	37°19.0′
	38	Changwu	CW	107°48.6′	35°1.8′
	39	Luochuan	LC	109°31.0′	35°38.6′
	40	Tongchuan	TC	109°4.9′	34°54.8′
	41	Wugong	WG	108°13.8′	34°5.1′
	42	Yaoxian	YX	108°59.9′	34°45.9′
	43	Taiyuan	TY	112°34.7′	37°35.9′
	44	Lishi	LS	111°7.4′	37°19.0′
	45	Yangquan	YQ	113°34.9′	37°39.9′
Shanxi	46	Yushe	YS	113°0.8′	36°53.1′
	47	Xixian	XiX	110°58.4′	36°31.3′
	48	Jiexiu	JX	111°56.6′	36°51.1′
	49	Linfen	LF	111°31.5′	35°53.5′

	50	Changzhi	CZ	113°5.9′	35°52.5′
	51	Yuncheng	YunC	111°2.4′	34°51.9′
	52	Houma	HM	111°23.5′	35°28.6′
	53	Yangcheng	YangC	112°25.7′	35°18.7′
	54	Youyu	YY	112°28.7′	39°48.0′
	55	Datong	DT	113°21.9′	39°54.0′
	56	Hequ	HQ	111°10.4′	39°11.3′
	57	Mount Wutai	WT	113°32.9′	38°45.4′
	58	Wuzhai	WZ	111°50.5′	38°43.4′
	59	Xingxian	XingX	111°9.4′	38°16.6′
	60	Yuanping	YP	112°44.7′	38°32.5′
Henan	61	Mengjing	MJ	112°27.7′	34°39.9′
	62	Sanmenxia	SMX	111°13.4′	34°37.9′

2

3

Table S2. *CONTRIBUTION*_GFGP (%) in 28 quadrats at 24 × 24 km scales from 2002 to 2015.

Quadrats	2005	2006	2007	2008	2009	2010	2011	2012	2013	2014	2015
CW					2.89	6.56	18.00	32.75	39.75	40.27	42.97
DB					4.23	7.58	11.54	38.67	50.55	52.43	52.53
EJH							1.12	2.17	19.92	33.88	40.47
GY							1.53	5.84	7.95	10.88	18.10
HN						7.33	15.38	20.35	33.43	42.18	44.68
HQ							1.28	3.39	4.52	10.23	15.42
HS				5.31	17.33	25.45	42.26	53.60	62.89	70.71	73.60
HX				6.09	19.61	32.21	52.78	60.29	58.43	61.09	65.38
HY				7.10	23.30	55.81	68.77	81.27	81.21	80.21	82.04
JY							12.84	41.64	61.42	60.44	62.55
LC				2.57	5.27	8.24	16.58	30.07	36.80	40.77	46.16
LS					1.69	5.14	9.43	14.17	19.80	25.25	29.21
LT			2.30	25.83	27.58	27.69	34.31	43.21	49.25	58.44	64.49
SD		44.57	59.78	75.97	87.08	92.54	92.15	88.81	79.00	79.01	81.26
TS						7.29	11.92	24.27	30.15	36.31	41.65
TX			10.55	48.72	53.97	65.37	82.22	87.72	87.25	82.50	81.17
WQ					2.90	14.22	22.48	31.67	37.23	42.61	45.16
XF					0.99	2.68	3.55	3.39	5.89	7.82	7.91
XingX	5.21	5.39	2.31	12.72	33.84	54.83	67.39	71.10	65.28	69.05	69.07
XJ							1.02	4.25	13.78	23.65	31.35
YanC					54.18	84.66	89.54	93.06	97.47	98.35	96.01
YL					1.87	4.35	8.84	16.40	19.08	30.16	35.18
YY						5.17	10.11	26.14	37.33	43.56	46.33
ZW							4.81	6.53	12.93	22.02	28.96

6